

CONF-9004139--1  
LBL-28294

Received by OSTI

MAR 13 1990



# Lawrence Berkeley Laboratory

UNIVERSITY OF CALIFORNIA

## Materials & Chemical Sciences Division

To be presented at the Poland Steel Meeting,  
Krynica, Poland, April 23-26, 1990, and  
to be published in the Proceedings

### Design and Processing of Strong-Tough Microcomposite Steels

Gareth Thomas

December 1989

DU NOT MICROFILM  
COVER



## **DISCLAIMER**

**This report was prepared as an account of work sponsored by an agency of the United States Government. Neither the United States Government nor any agency thereof, nor any of their employees, makes any warranty, express or implied, or assumes any legal liability or responsibility for the accuracy, completeness, or usefulness of any information, apparatus, product, or process disclosed, or represents that its use would not infringe privately owned rights. Reference herein to any specific commercial product, process, or service by trade name, trademark, manufacturer, or otherwise does not necessarily constitute or imply its endorsement, recommendation, or favoring by the United States Government or any agency thereof. The views and opinions of authors expressed herein do not necessarily state or reflect those of the United States Government or any agency thereof.**

---

## **DISCLAIMER**

**Portions of this document may be illegible in electronic image products. Images are produced from the best available original document.**

Gareth Thomas

DE90 007764

Professor, Dept. of Material Sciences and Mineral Engineering, University of California, and Scientific Director, NCEM, LBL, Berkeley, CA 94720.

## ABSTRACT

Microcomposite HSLA steels based on Fe/Cr/Mn/C have been designed as a result of sophisticated electron microscopy and microanalytic studies so as to consist of fine packet lath dislocated martensite and interlath austenite films in order to obtain steels with superior combinations of strength, fracture toughness, and formability. Such properties can be obtained directly by on-line controlled rolling and cooling directly in a hot mill, so that post tempering can be eliminated. For long products and plates of low to medium carbon compositions, the processing requires accelerated water cooling. Niobium is effective in increasing hardenability, in grain refinement, and without adversely modifying the microcomposite morphology of the steels.

## 1. INTRODUCTION

## 1. A. Microstructural basis of alloy design for high strength, tough structural steels.

This paper represents a review and summary of the microstructural design and processing programs that have been underway at Berkeley over the past twenty years or so for improving the mechanical properties of HSLA steels from first principles. The overall objective has been to blend physical and process metallurgy to achieve economical but superior microcomposite steels of high strength, toughness and other desirable properties. The original research has been published in a series of papers and conference reports, e.g., refs. 1-8.

Attention has also been paid to methods of processing these steels by controlled rolling and cooling to simulate actual hot mill practice. In this way conventional methods involving subsequent quenching and tempering could be eliminated. That is, the desired microcomposite microstructure is produced directly on line in the finished product thereby eliminating costly tempering treatments.

High strength structural steels are used extensively for components such as aircraft landing gear, forged bars, missiles, rocket casings, armor plate, and other defense applications. In addition, where steels have high hardness and consequent abrasion resistance, they are used in mining operations (for example, in chains, as buckets) and in comminution and mineral processing operations. The limiting factor in the use of high strength

steels is their toughness. In practice, toughness and ductility are required to resist crack propagation (i.e., have high  $K_{IC}$  values) and ensure sufficient formability for successful fabrication of the steel into engineering components. Many commercial high strength steels in use today have been designed by experience, often by trial and error, and almost all of those at high strength levels could benefit from improvements in toughness. It is unfortunate that several problems have arisen with high strength steels due to inadequate attention being paid to their fracture toughness, (e.g., rocket failures, aircraft disasters, ships and bridge failures, etc.), which have occurred in strong but brittle steels of low  $K_{IC}$ . Some examples are shown in figs. 1,2.

Since the  $K_{IC}$  property is microstructure sensitive it is clear that much research can be done to improve the fracture toughness so that high strength steels may be used with higher integrity. With this objective in mind, a systematic study of the relation between martensitic (and bainitic) microstructures and properties utilizing a series of Fe-C-X high purity, vacuum melted experimental steels (where X is the substitutional solute) has now been completed.<sup>(1)</sup> The martensite transformation, if controlled so that the inhomogeneous shear component occurs by slip and not by twinning, is one of the most efficient means of producing dense, uniformly dislocated, fine grained structures.<sup>(3)</sup> Figure 3 shows that at similar yield strengths, twinned carbon steels are far less tough than dislocated martensitic steels. Dislocations are an essential component for strength and toughness. The main factor controlling this aspect of the transformation is composition, especially carbon (and/or nitrogen) content (affecting transformation temperature  $M_s$  and strength of martensite), which must be regulated to maintain  $M_s > 200^\circ\text{C}$ . This sets the upper carbon (and nitrogen) limit to about 0.35 wt.% as can be seen from fig. 4. It is clear that  $M_s$  temperature is an important design parameter in these studies, and attention has been paid to this point in the present research program.<sup>(10)</sup> Data collected from the literature especially for binary alloys (after Izumiyama<sup>(11)</sup>) are shown in fig. 4 (a). Figure 4 (b) summarizes a plot of all the observed  $M_s$  values obtained over the years of research on our steels fitted to the equation of Andrews<sup>(12)</sup>. Similar results apply to the equation of Steven and Haynes<sup>(13)</sup>. Both equations are satisfactory for estimating  $M_s$  temperatures for the composite lath martensite-austenite steels of interest in the present work, although some modifications may apply to high Cr and Mo alloys.<sup>(10)</sup> Thus a steel may be designed mainly on the basis of  $M_s$  so as to give the microcomposite structure using a wide range of suitable alloying elements. However, chromium remains one of the most useful and economical alloying elements available today.

It has also been possible as a result of detailed analyses by electron microscopy and diffraction, to show that retained interlath austenite films in the martensite packets promotes increased toughness to crack propagation.<sup>(3-8)</sup> Thus, the microstructure which corresponds to optimum mechanical properties is a microcom-

posite duplex austenite-martensite structure in which packets of laths contain stable inter-lath austenite films, (fig. 5 a-d). These structures exhibit Kurdjumov-Sachs orientation relationships.<sup>(6)</sup> Thus, since each packet corresponds to laths of a particular (111) $\gamma$  variant, (fig. 5 b) the maximum number of variants in a prior austenite grain is four, although several packets of martensite of the same variant can be present.<sup>(14)</sup> These packets can thus be refined by controlled hot rolling, so as to recrystallize austenite for maximum grain refinement. The excellent combinations of strength and toughness exhibited by the steels so developed, even in the untempered condition, can be seen in the summary results in fig. 6.

The temperature limitations of applicability of these steels is in the 300<sup>o</sup>-400<sup>o</sup>C range since this leads to tempered martensite embrittlement (fig. 7). This phenomenon has been shown to occur by decomposition of the interlath retained austenite<sup>(6-8)</sup> to interlath carbides (figs. 7-8). The austenite stability is related to the behavior of carbon and substitutional atoms in partitioning. Studies of such phenomena have required the application of the most advanced microanalytical techniques such as convergent beam electron diffraction and field atom probe spectroscopy. Such methods are summarized in figure 9. More details are given in refs. 8, 14, 15.

#### 1. B. Alloy Compositions and Processing

The present research has studied individually and collectively the roles of C, Cr, Mn, Ni, Mo, Ti and others on the microstructure-property relations of Fe base alloys. A wide range of alloys has now been developed based on the Fe/Cr/C system.<sup>(16)</sup> Typical compositions of the most recently developed alloys<sup>(17)</sup> for long products and/or plates are given in Table 1. Here the emphasis has been concerned with lean compositions (e.g. Cr at 1-2% with 1% Mn for retained austenite) to develop the desired microcomposite microstructures on line in a steel plant by controlled hot rolling and (accelerated) cooling. The processing is shown schematically in fig. 10 for air hardenable (10%) and water quench hardenable (2%Cr) alloys. However, in lean compositions, limits on hardenability will require rapid quenching rates, of the order of 40<sup>o</sup>C/sec, depending on final product thickness, in order to produce the desired autotempered packet martensite and to avoid interlath carbide precipitation or other unwanted austenite decomposition products during the quench. In actual plant operation rapid quenching rates are difficult to achieve and require enormous quantities of water. A practical limit on quench rate is about 30<sup>o</sup>C/sec. However, the addition of a small amount of Nb (e.g., 0.02 wt % Nb) to Fe/2Cr/1Mn/0.25C alloys has been successful in reducing the stringent quenching conditions, by an increase in hardenability (fig. 11) whilst allowing a fine austenite grain size to be obtained during controlled hot rolling just above the recrystallization temperature.<sup>(17)</sup>

The usual microalloying principle used for low carbon steels is to control roll, usually below the austenite recrystallization

temperature, to develop pancake shaped grains. The grain size is controlled by forming microalloyed carbides or carbonitrides at ferrite grain boundaries, so reducing grain growth. (18,19) The resultant steels show excellent Charpy (crack initiation) toughness but because of the grain boundary precipitates often give poor  $K_{IC}$  toughness values, i.e., poor crack propagation resistance. (20,21) In the present scheme a different approach is used whereby the controlled rolling is done by finishing just above the austenite recrystallization temperature to produce a fine grained austenite which is then directly quenched to produce a fine micro-composite packet martensite-austenite structure. These comparative approaches are schematically shown in fig. 12. In actual plate trials conducted by Dillinger-Huttenwerke (W. Germany) plates of Fe/2Cr/1Mn/0.26C/ 0.26 Nb were controlled rolled and quenched at 30°C/sec. to between Ms-Mf to obtain on-line autotempering. The results showed remarkably high toughness (Charpy > 90 joules) as plotted in fig. 6 and are even better than those obtained in the laboratory (tables 2,3). Figure 13 shows a plate on the water cooling table following finish hot rolling.

A further processing route (fig. 14) has been investigated for rounds, in which these low alloy steels were controlled rolled (as in Fig. 10), followed by normalizing rather than quenching, so that the steels are easily spheroidised to be cold formable. For these applications Nb additions may not be necessary. (17) Such processing follows the current technology to produce products such as bolts, chains, etc. (fig. 15). The final product is subsequently quenched and tempered to achieve the same strong-tough microcomposite structure as indicated above. Some properties from these processing routes are shown in fig. 16 a-c (from ref. 17). As can be seen from the above, this research program involves physical and mechanical metallurgy principles with emphasis on control of microstructure and composition. The following briefly summarizes the main experimental methods which have been utilized in the laboratory developments in this program.

## 2. Experimental Procedures

The experimental designed alloys ranging from 1-10%Cr, 1-2%Mn, 0.1-0.4C and other elements e.g., Nb, and Mo etc. were vacuum melted as 30 Kg ingots and subsequently forged to 75 mm thick, 75 mm wide and 330 mm long billets. These were then homogenized at 1200°C for 24 hours in a vacuum furnace before cooling. The compositions given in Table 1 were measured after homogenization. Billets were cut into 40 mm thick, 38 mm wide and 76 mm long blanks, into which thermocouples were embedded to read the exact temperature during rolling. They were austenitized at 1100°C-1200°C for 75 minutes in a horizontal furnace. Controlled rolling was conducted on the austenitized blanks as shown in fig. 10. The first rolling of 30% reduction was done at 1100°C. The second finishing rolling was done at 950°C, 900°C and 850°C, respectively with a total reduction of 45 %. The cooling rate

was also varied using quench media of water or agitated oil or by releasing in the air after controlled rolling. Isothermal tempering treatments were done at 200°C and 250°C, and by arresting the quench after rolling in the same temperature range. (22) These results were compared with steels given conventional quench-temper treatments (6) rather than the control-rolling/cooling procedures. (1,17) Standard ASTM size specimens were used to measure the Charpy V-notch impact energy (the long axis of the test specimens was parallel to the rolling direction, and the base of the notch was perpendicular to the surface). Testing was conducted with a 224 ft-lb capacity impact machine at room temperature. Broken impact specimens were then examined for fractography in a scanning electron microscope operated at 25 Kv. The 31.5 mm gauge round tensile specimens were pulled at cross head speed of 0.3 mm/min at room temperature.  $K_{IC}$  fracture toughness measurements were also done out using ASTM standards. (6)

Microstructural examinations were conducted by optical and transmission electron microscopy (TEM) techniques. Thin foils for TEM were obtained from broken fracture test specimens in the usual way involving final electropolished in a twin jet electropolishing apparatus at -2°C in a perchloric acid - ethanol - glycerol solution at a voltage range of 12 to 15 volts and current range of 18 to 20 milliamperes. Transmission electron microscopy, microdiffraction and microanalyses were carried out routinely on all samples. In addition, spectroscopy by field ion atom probe methods (8,15) was also utilized to obtain microanalyses of the austenite and lath martensite. The continuous cooling transformation diagrams were obtained by the dilatometry method using various cooling rates, and an example for the two alloys listed in Table 1 is shown in fig. 11, (courtesy ref. 17).

### 3. Results

#### A. Mechanical Properties

The mechanical properties of the low chromium (2%) steels with and without niobium, (17) laboratory processed as in figs. 10, 12 are summarized in Tables 2 and 3. Tensile strength and Charpy toughness depend on finish rolling temperatures and cooling rate and an example is plotted in Fig. 16. As fig. 17 shows, the niobium bearing steel shows a great improvement in impact toughness compared with the non-Nb quaternary alloy by about 15 joules. This is attributed to the effect of niobium on grain refinement. Finish rolling at 850°C or lower results in lowering of the Charpy impact energy because of rolling below the recrystallization temperature. Tempering at 200°C also contributes to the increment of Charpy impact energy. Therefore, such a rolling schedule can result in a higher impact toughness in an actual steel mill without conducting any subsequent temper treatments. This practice of course only applies to finished products - essentially the same process could be used for hot forging and control cooling. Figure 6 summarizes the data for all steels tested both in laboratory and steel mill trials, and compared

with some commercial steels.

## B. Microstructure and microanalysis

Electron microscopy has shown that all steels processed by the above methods contained the desired microcomposite lath martensite (autotempered or tempered) with interlath retained austenite films (e.g., fig. 5c), which are stable on tempering up to 300-400°C depending on composition, as has been published previously. The results of the detailed microanalytical studies (fig. 9) have shown that over 7 at % carbon partitions to the austenite. (8, 15) This phase is thus stabilized both by carbon (very low  $M_s$  temperature) and mechanically (thin film morphology).

## 4. Discussion

### 1. Toughness

It is important to recognize the differences between crack initiation (Charpy toughness) and crack propagation ( $K_{IC}$ ) toughnesses. These properties often appear to relate inversely, as when considering grain size effects (20) and austenitizing temperature e.g., so as to obtain all carbides in solution (21). In designing for toughness against crack propagation, high  $K_{IC}$  values are required. A simple relation exists between critical flaw size  $a_c$ , stress, and  $K_{IC}$  as follows:-

$$a_c = \frac{1}{1.2\pi} [K_{IC} / \sigma]^2$$

This relationship is plotted in fig. 18 for three steels having a similar yield strength but with different  $K_{IC}$  values. For a critical crack size of 0.25 cm, it is clear that the microcomposite steels processed as described above and which can easily obtain  $K_{IC}$  values of 100 MPa $\sqrt{m}$  and hence can tolerate such a crack up to the yield limit. However, typical commercial steels can only tolerate such a crack at stresses to only about 30% of the yield strength. This was the problem with the failure shown in fig. 1 in which the  $K_{IC}$  is estimated (9) to be only 54 MPa $\sqrt{m}$ . The advantage of the designed microcomposite microstructures for improved fracture tolerance is quite apparent.

A model for the improved toughness of these designed microcomposite microstructural steels has been proposed earlier. (7,15) The coherent or semi-coherent austenite-lath martensite interface, as is well known from the Kurdjumov-Sachs (K-S) crystallographic relationships for these microstructures, allows slip to cross both phases so that large plastic zones can be sustained ahead of growing cracks. If, however, there is no "buffer" film of austenite, but rather interlath carbides, only a small plastic zone is possible and hence, low  $K_{IC}$  values are to be expected. Thus, the path of growing cracks will be determined by the morphology of the microcomposite structure (fig. 7-9). Mechanical stability of the austenite is also important. (6) Silicon has been found to

destabilize austenite near high stress fields, e.g., at crack tips. The austenite then transforms to high carbon twinned martensite which is also embrittling. Thus, silicon is not recommended as a deoxidiser, but rather Al. Also, since austenite has a high solubility for many elements, e.g., H<sub>2</sub>, these steels may be quite tolerant to impurities, as a result of solid solution capabilities of the untransformed austenite.

## 2. Compositions

In practice, a range of desired mechanical properties such as strength, toughness fatigue and hardness values can be manipulated by modifying composition to the desired M<sub>s</sub> (fig. 4). The control rolling should be done just above the austenite recrystallization temperature and the cooling rate should be fast enough to avoid bainitic reactions. In order to obtain the desired microcomposite microstructures, the following summary applies. The Cr range varies from 2-12% with the high Cr values being designed for improved corrosion resistance, e.g., in precious metal mining conditions where the environment is very acid. These high chromium steels are air hardenable to 40 cm thickness and so are easily mill processed. (23) Strength and hardness is determined mainly by carbon (and/or nitrogen) content, and Mn, which is more economical than Ni, helps in stabilizing the interlath austenite, (1-8) in addition to adding hardenability. Thus, when Mn is considered for desulphurizing it must also be sufficiently concentrated to obtain the retained austenite. Molybdenum, where necessary is also beneficial for strength and temper resistance (6,14). By increasing carbon it may be possible to achieve very much higher combinations of hardness and toughness than are available at present. However for good toughness it is necessary to avoid excessive twinned plate martensite so the final M<sub>s</sub> temperature must be  $\geq 200^{\circ}\text{C}$ . Solution treatments at about  $1150^{\circ}\text{C}$  are suitable for these Fe/Cr/Mn/C steels since iron and chromium carbides are not difficult to dissolve (unlike other alloying elements, e.g., Ti). (21) For the Nb bearing steels soaking at  $1200^{\circ}\text{C}$  is needed. (17)

## 3. Other Properties

In addition to strength and toughness many of the uses of structural steels require many other engineering properties. Examples include fatigue<sup>(1)</sup>, wear, corrosion resistance etc. Both sliding and abrasive wear behavior have been examined and measured for these microcomposite steels. (24-28) The results show that the duplex martensite/austenite microstructures exhibit good wear-resistance in both categories of wear, and are superior to many commercial alloys that are utilized as wear-resistance alloy. Also, the sliding wear behavior of these steels has been further enhanced by laser surface hardening. (27) Using a 500 watt, continuous CO<sub>2</sub> laser, localized, rapid heating and quenching can be confined to the surface of the alloys, producing a hard, grain-refined microstructure to depths of 500 microns and hence, a two-fold increase in wear resistance. Consequently, materials with a fine-scale microstructure and a high yield strength in the

absence of large undeformable particles, appear to be the most wear resistant.

## 5. Summary

In order to meet production hot mill plant requirements, plants with no accelerated cooling facilities will require air-hardenable steels so as to obtain on-line the desired microstructure (fig. 5 ), e.g., Fe/10Cr/1Mn/0.2C (16, 23). However, it must be emphasized that even in regular steel plants without water cooling if steels are control rolled so as to maximise austenite grain refinement they can still be produced with superior properties (e.g., processed as in fig. 14 RHS) if the final structures are the microcomposites discussed herein. For plants with water cooling capabilities typical practical quench rates that can be obtained are of order  $\sim 30^{\circ}\text{C}/\text{sec}$ . In this case the leaner alloys such as the Fe/2Cr/1Mn/0.25C/0.02Nb compositions are suitable for final thicknesses up to 25-30 mm. In the latter case, by controlling the finish roll temperature and cooling rate, with arresting the quench above  $M_f$ , so as to allow auto tempering it is possible in a commercial hot mill to achieve the composite microstructures and properties on-line without subsequent tempering. This approach can be important for many applications and represents potential cost savings compared to post rolling heat treatment procedures. Of course, subsequent tempering will always raise the toughness. The specific alloy and procedures adopted depend on the properties and applications desired.

## ACKNOWLEDGEMENT

This work was supported by the Director, Office of Energy Research, Office of Basic Energy Sciences, MCS Division, of the U.S. Department of Energy, under contract No. DE-AC03-76SF00098. Thanks are due to all the researchers and graduate students who have been involved in this project for the past 15-20 years. Steels have been provided by various companies, notably Allegheny-Ludlum, ISCOR, South Africa, and Posco, S. Korea. Joint research in cold forming and applications of the microcomposite steels with R. Milovic of Boris Kidric Steel Works, Niksic, Yugoslavia is also acknowledged. The cooperation of ISCOR, and Dillingen (West Germany) for plant trials, and for making their data available is very much appreciated.

## References

1. G. Thomas, ICMSR 89 Conf. Beijing, China, Int. Acad. Pubs. 63, 1989.
2. G. Thomas, Fundamental Aspects of Structural Alloy Design, R.I. Jaffee, and B.A. Wilcox, eds. Plenum Press, NY., 33, 1977.
3. G. Thomas, J. Int. Iron and Steel, 46 451, 1973.
4. G. Thomas, Design of Strong, Ductile, Duplex Low Alloy Steels, N.R. Comins, and J.B. Clark, eds. Conf. Proc. on Speciality Steels and Hard Materials, Pretoria, S. Africa 55, 1983.
5. G. Thomas, Metall. Trans. 9A 439, 1978.
6. B.V.N. Rao and G. Thomas, Metall. Trans. 11A, 441 1980.
7. M. Sarikaya, A. Jhingan, and G. Thomas, Metall. Trans. 14A, 1121 1983.
8. G. Thomas, M. Sarikaya, S.J. Barnard, and G.D.W. Smith, Advances in Physical Metallurgy of Steels, Inst. of Metals, London, UK, 259, 1983.
9. J.E. Srawley and J.B. Esgar, NASA Rm-x-1194 1967.
10. C.Y. Yung and J.J. Rayment, Met. Trans., 13A, 328, 1982.
11. M. Izumiyama, M. Tsuchiya and Y. Imai, J. Jap. Inst. Met., 34, 291, 1970.
12. K.W. Andrews, J. I.S.I. S203, 721, 1965.
13. W. Steven and A. G. Hayes, *ibid*, 183, 349, 1956.
14. M. Sarikaya, B.G. Steinberg, and G. Thomas, Met. Trans. 13A, 2227, 1982.
15. M. Sarikaya, G. Thomas, J.W. Steeds, D.J. Barnard, and G.D.W. Smith, Proc. Int. Conf. Sol. State Phase Trans. ASM (ed. H.I. Aaronson), 1421, 1982.
16. J.A. McMahon and G. Thomas, Proc. Int. Conf. on Microstructure and Design of Alloys, Inst. of Metals, London, UK, 1, 180, 1973.
17. G. Thomas, J.K. Kim, D. Manojlovic and R. Milovic, Proc. Int. Conf. of HSLA Steels, Pittsburgh, PA 11/88, Met. Trans.-AIME, (ed. A.J. de Ardo), 399, 1988.
18. T. Tanaka, Int. Met. Rev. No. 4, 185, 1981.
19. Proc. 8th Process Technology Conf. Dearborn, MI, 1988 (eds. J.E. Hartmann, M. Korchynsky and A.J. de Ardo), ISI-AIME, Warrendale, PA, USA 1989.
20. R.M. Horn and R.O. Ritchie, Met. Trans. A. 9A, 439, 1978.
21. M.F. Carlson, B.V. N. Rao and G. Thomas, Met. Trans. 10A, 1273, 1979.
22. On-line plant trials have been successfully carried out at Dillinger-Huttenwerke, West Germany (on plates) using the process scheme of fig. 10 with water cooling at  $-30^{\circ}\text{C}/\text{sec}$  (fig. 13). I am grateful to Dr. J. Humbert and his colleagues for their cooperation in this effort.
23. R. Ramesh and G. Thomas, Met. Trans., in press.
24. W.J. Salesky, R.M. Fisher, G. Thomas, and R.O. Ritchie, Wear of Materials, (ASME), 434, 1983.
25. C.K. Kwok and G. Thomas, *ibid.*, 140.
26. C.K. Kwok and G. Thomas, *ibid.*, 612.
27. J. Kusinski and G. Thomas, Proc. S.P.I.E. 668, 150, 1986.
28. Y. Yoon and G. Thomas, Int. Symp. on the Plasticity and Resistance to Metal Deformation, Herceg, Yugoslavia, 64, 1986.

Table 1. Alloy Compositions

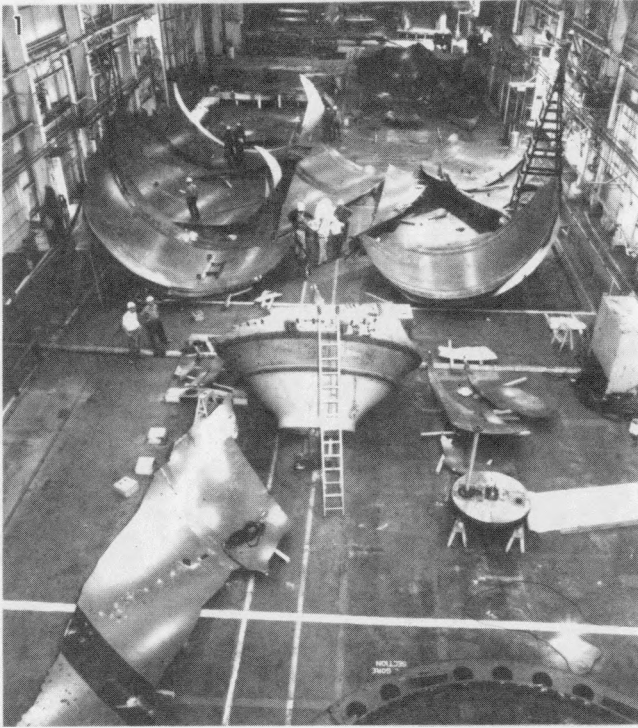
Alloy	C	Mn	Cr	Nb	Si	P	S
Non Nb Steel	0.26	1.20	1.99	-	0.14	0.012	0.015
With Nb Steel	0.24	1.21	1.98	0.02	0.046	0.006	0.004

Table 2. Mechanical Properties of Fe/0.25% C/1.2% Mn/2.0% Cr

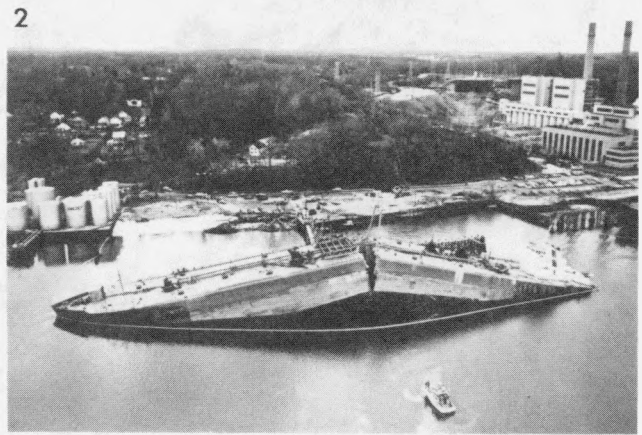
First Rolling Temp(°C)/Red(%)	Second Rolling Temp(°C)/Red(%)	Tempering Temp(°C)	YS (MPa)	UTS (MPa)	Elongation Total(%)	Charpy Impact Energy(J)
1100/30	950/45	As-WQ	1208	1630	12.6	33
		200				38
		250	1236	1505	14.7	35
		As-OQ	1139	1608	15.4	29
		200				33
	250	1236	1498	16.8	31	
	Air Cool	842	1188	15.4	4	
	900/45	As-WQ	1374	1601	13.3	29
		200				35
		250	1111	1456	13.3	34
		As-OQ	1208	1601	16.8	26
		200				31
	250	1236	1519	15.4	29	
	Air Cool	739	1111	18.2	4	
	850/45	As-WQ	1456	1769	10.2	15
200					19	
250		1312	1658	15.4	19	
As-OQ		1236	1760	15.4	15	
200					24	
250	1284	1637	14.7	22		

Table 3. Mechanical Properties of Fe/0.25% C/1.2% Mn/2.0% Cr/0.02% Nb

First Rolling Temp(°C)/Red(%)	Second Rolling Temp(°C)/Red(%)	Tempering Temp(°C)	YS (MPa)	UTS (MPa)	Elongation Total(%)	Charpy Impact Energy(J)
1100/30	950/45	As-WQ	1139	1540	16.1	46
		200				52
		250	1188	1485	16.1	41
		As-OQ	1126	1512	16.1	42
		200				46
	250	1208	1485	16.8	41	
	Air Cool	842	1091	19.6	4	
	900/45	As-WQ	1138	1560	16.8	38
		200				46
		250	1188	1540	16.8	35
		As-OQ	1160	1519	16.8	48
		200				54
	250	1160	1485	15.4	42	
	850/45	As-WQ	1160	1540	14.7	35
		200				41
250		1340	1512	14.0	31	



XBB 688-4968

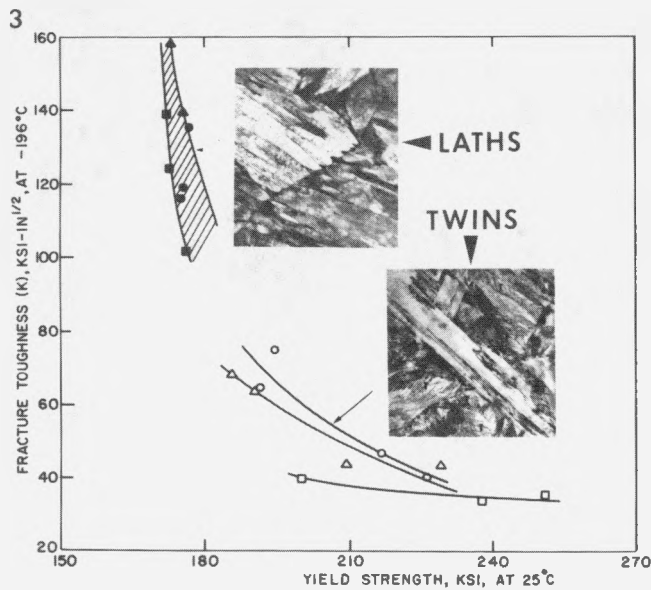


XBB 821-125

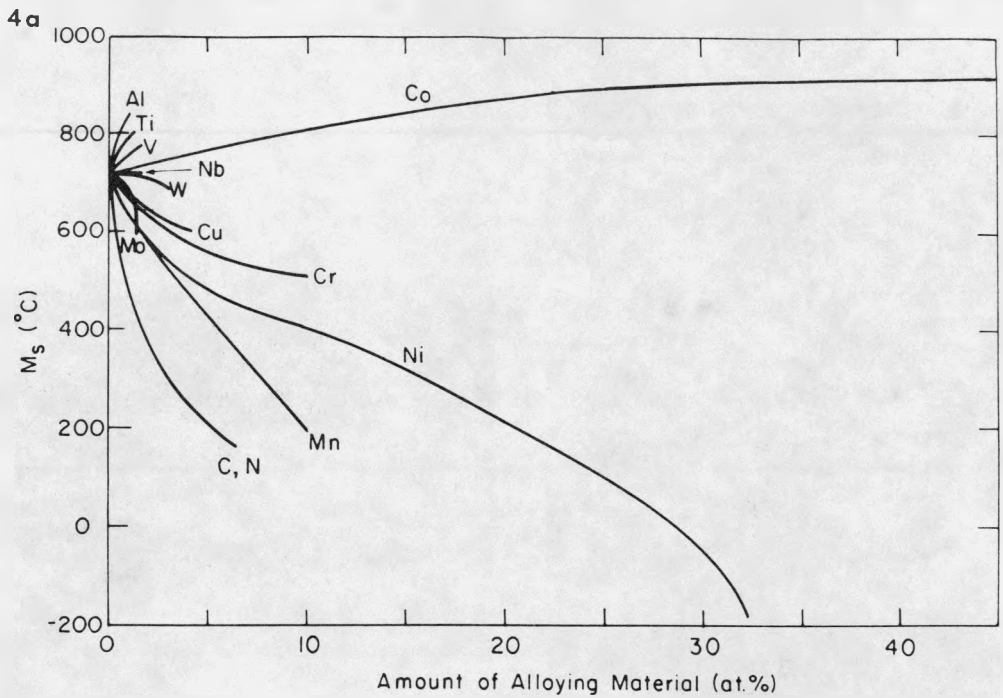
Fig. 1 A 250 grade maraging steel rocket casing, brittle fracture at weldments (ref. 9).

Fig. 2 Ductile-brittle fracture of high strength carbon steel plates in a cargo ship.

Fig. 3 Showing the fracture toughness-strength relationship in a variety of quenched and quenched and tempered steels. Notice the lower toughness at the same yield strength when the martensitic microstructure is in the twin plate form (inset electron micrograph).



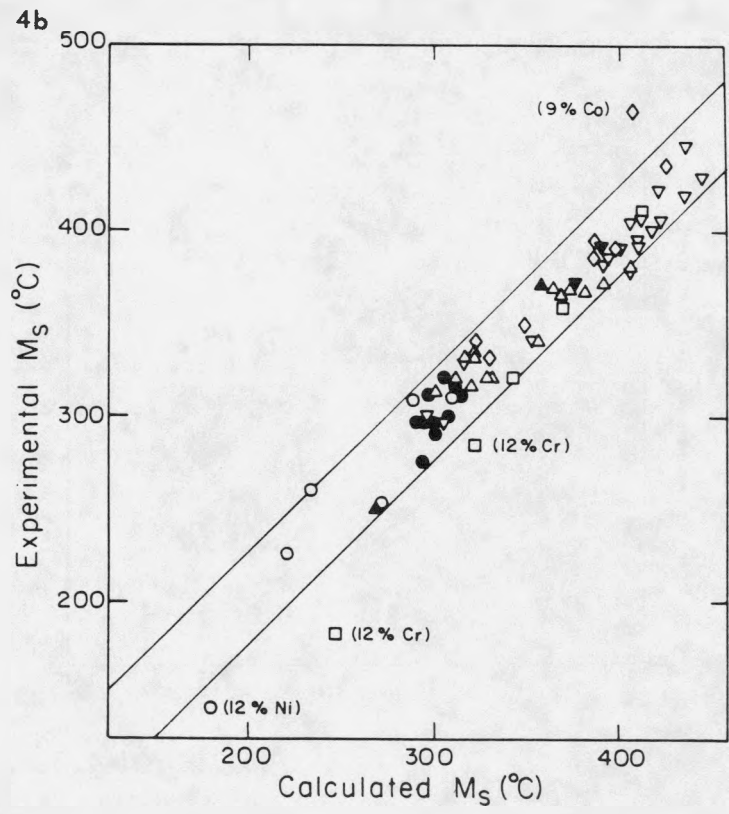
XBB 701-475



XBL 812-5140

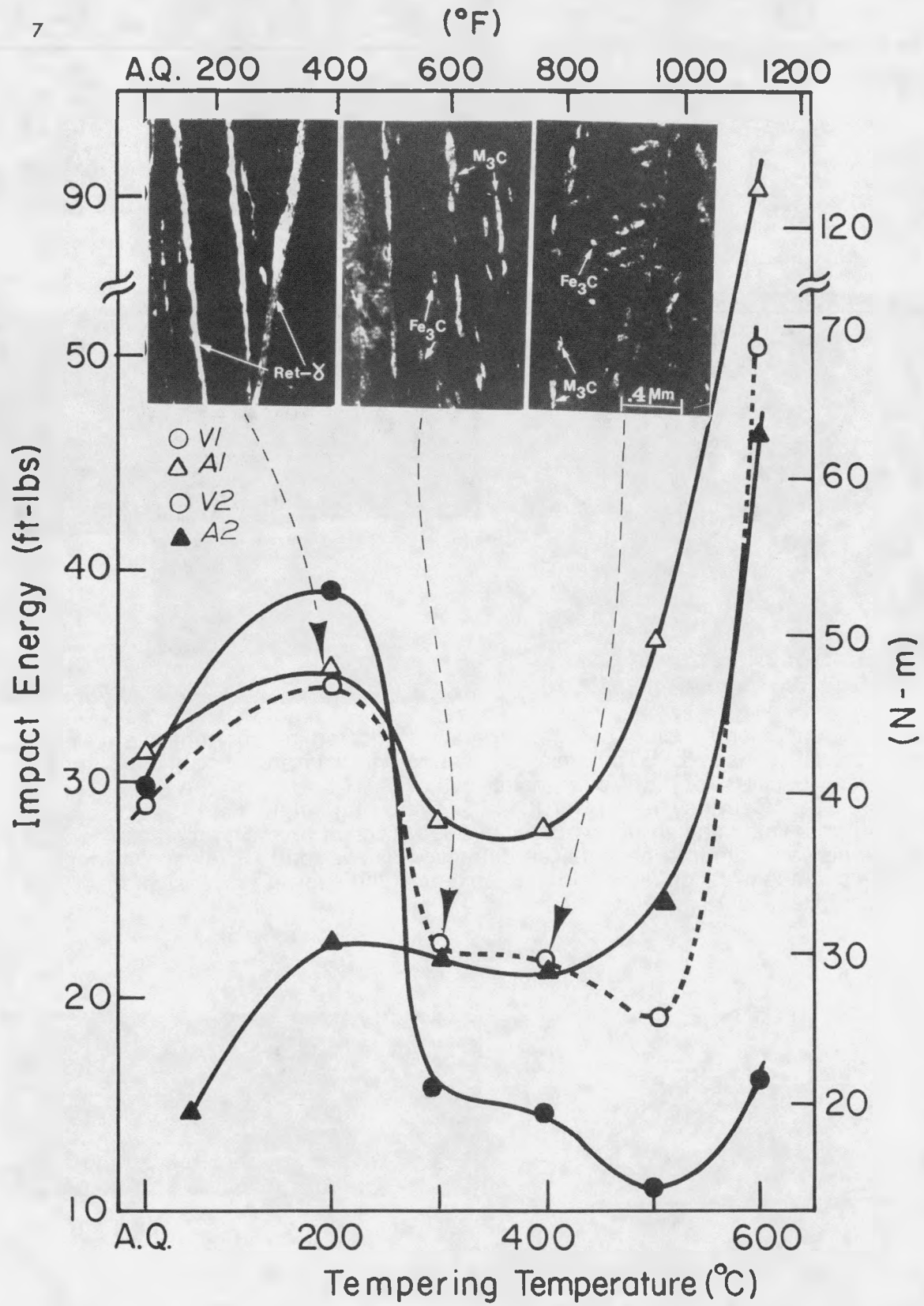
Fig. 4(a) Martensite start temperatures for binary iron base alloys. (from Izumiyama et al., ref. 11)

Fig. 4(b) Comparison of experimental, measured, and calculated  $M_s$  data (ref.10). The measured data refer to values from steels developed in the Berkeley microcomposite steel program based on Fe/Cr/Mn/C. Calculated results using Andrews' non linear equation (ref. 12).



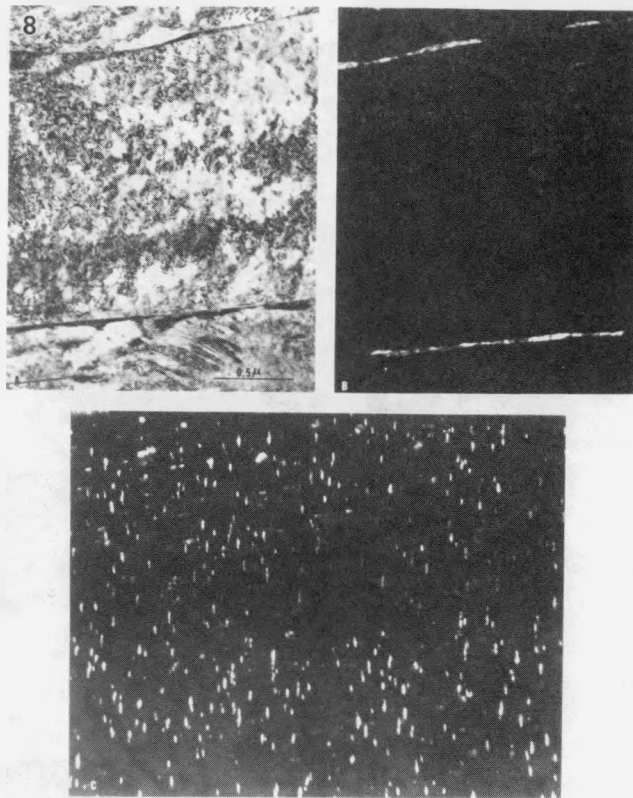
XBL 817-10731





XBB 821-4

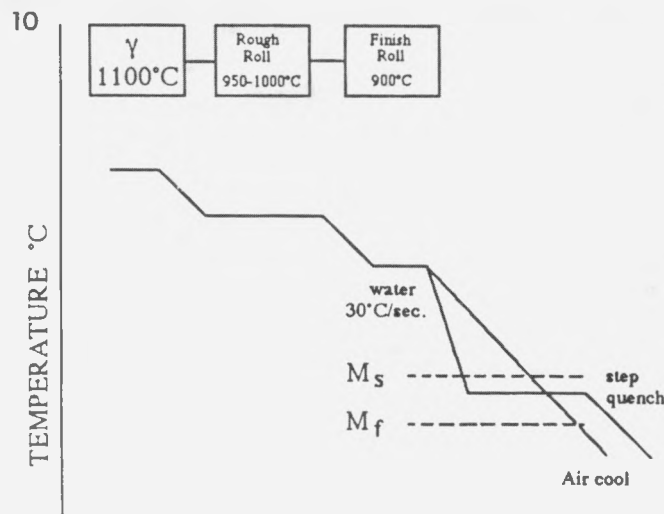
Fig. 7 Microstructure-Charpy impact energy relations for post tempered Fe/3Cr/2Mn/0.26C steels. TME associated with interlath austenite decomposition to carbide. (Courtesy ref. 7)



XBB 720-5615

Fig. 8 Bright and dark field imaging to show the intralath carbide has no crystallographic relation to the interlath carbide formed by interlath austenite decomposition on tempering ~ 400°C (as in fig. 7).

Fig. 10 Schematic of control rolling/cooling processing procedures. Cooling rate on line of 30°C/sec is required for alloys shown in Table 1.



Recommended processing for on-line hot mill products such as plates, rounds, and sections. If subsequent processing is required for W.Q. alloys, steels can be normalized from finish rolling temperature, processed, then quenched 900° C and tempered 225° C.

XBL 8810-3730

# CARBON PARTITIONING IN RETAINED-AUSTENITE IN LATH-MARTENSITIC STEELS

## TRANSMISSION ELECTRON MICROSCOPE - IMAGE STUDIES

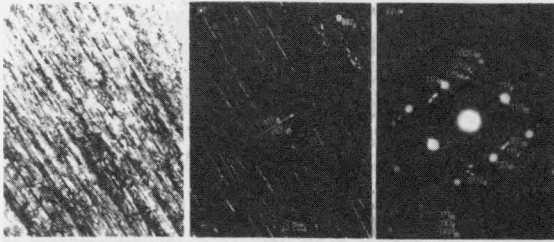
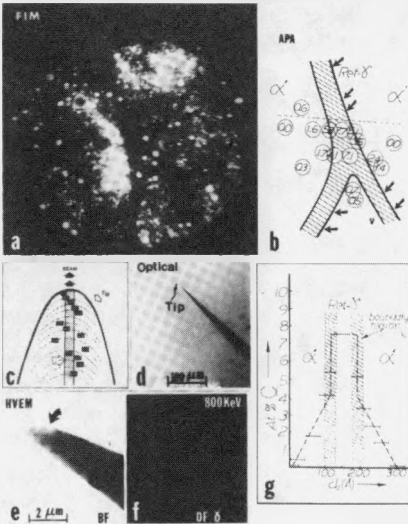


FIGURE 1 - (a) and (b) of  $(002)_\gamma$  images illustrating the general appearance of thin films of Ret- $\gamma$  at the martensite lath boundaries (0.5 at.% C steel). (c) Composite SAD pattern of martensite (M) and austenite (A).

The microstructure consists of dislocated lath martensite with fairly straight boundaries and thin film Ret- $\gamma$  at the lath-like martensite crystal boundaries. DF micrographs (fig. 1) shows an extensive amount of Ret- $\gamma$  (5 vol.%) even at this low carbon level. The existence of this high temperature phase at low temperatures is attributed to several mechanisms in which interstitial C stabilizes the austenite. (i) Chemical stabilization: Diffusion and partitioning of C in Ret- $\gamma$  decrease the local  $M_s$  temperature and inhibit further transformation. (ii) Thermal stabilization: During quenching interstitial C forms dislocation atmospheres in  $\alpha'$  and at the  $\alpha'/\gamma$  interface, pinning the dislocations and suppressing interface motion. (iii) Mechanical stabilization: Part of the austenite to martensite shear transformation strains is accommodated by soft  $\gamma$ , which deforms extensively to prohibit the transformation.

The average C concentration in Ret- $\gamma$  can be determined by measurements of shift in positions of the holtz lines in CBED patterns in relation to the change in the lattice parameter of the Ret- $\gamma$ , due to C:  $(\Delta a/a_{ref}) = (2/3)[(p/q_\gamma) - (p_{ref}/q_{ref})](9/115)^{1/2}$ . Ni (99.99% with  $a_0 = 3.5238$ ) was used as a reference, and results cross-checked with Cu (99.999% with  $a_0 = 3.6150$ ). For the example shown in fig. 2, C at.-% =  $4.9 + 0.6$  (at.-% C alloy = 0.7) taking  $a_{Ret-\gamma} = 3.555 + 0.044X$  (w/o C).

## FIELD ION MICROSCOPY - ATOM PROBE ANALYSIS



Atom probe analysis provided direct quantitative determination of the C distribution in  $\alpha'$  and Ret- $\gamma$  at 20-30 Å resolution. Considerable C enrichment occurs in Ret- $\gamma$  - direct evidence of chemical stabilization (figs. 3-4). Detailed measurements of C distribution in a thicker Ret- $\gamma$  film (fig. 4) gave an average concentration of 3.0 at.%, and up to 8.5 at.% at the  $\alpha'/$ Ret- $\gamma$  interface (Thermal stabilization). The extent of deformation (Mechanical stabilization) is discernible in TEM micrographs in fig. 4. There is no apparent change in distribution of substitutional alloying elements (Cr and Mn, fig. 4) in  $\alpha'$  and Ret- $\gamma$ . Hence changes in the amount of Ret- $\gamma$  with alloying elements are attributed to their interaction with C influencing its mobility. Thus the overall stability of thin film Ret- $\gamma$  is due to effects of several mechanisms.

FIGURE 3 - (a) FIM image of Ret- $\gamma$ . (b) Regions of APA analysis. (c) Illustration of the analysis of subsurface regions by field evaporation. (d) Low magnification image of the tip. (e) HVEM image and (f) DF image reveal Ret- $\gamma$ . (g) Concentration profile for C across the interface.

Retained austenite (Ret- $\gamma$ ) has been identified in a number of carbon containing lath martensitic steels with  $M_s$  and  $M_f$  temperatures well above room temperature. Because of its beneficial effects on the mechanical properties (especially fracture toughness) of HSLA steels the influence of interstitial C in stabilizing the  $\gamma$  has been studied in detail using TEM, CBED and FIM-APA techniques.

Steels were austenitized at 1100°C, and oil quenched. TEM foils were prepared by electropolishing in chromic acid at room temperature (RT), and Cu and Ni standards in 25%  $\text{NH}_3$  in  $\text{CH}_3\text{-OH}$  at -30°C. Some steel foils were etched for CBED by "dipping" in 15%  $\text{HClO}_4$ -5%  $\text{C}_2\text{H}_5(\text{OH})_2$ - $\text{CH}_3\text{COOH}$  at -25°C. FIM tips were electropolished in 25%  $\text{HClO}_4$  in  $\text{CH}_3\text{-COOH}$  at RT.

## CONVERGENT BEAM ELECTRON DIFFRACTION

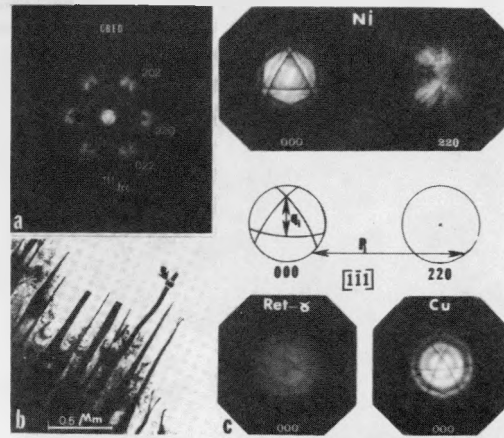


FIGURE 2 - (a) Nickel (fcc) 111 CBED-pattern at 100 kV reveals trigonal symmetry. (b) DF image from a specially prepared foil, shows the Ret- $\gamma$  films extending into the perforation. (c) Disc formed by forward scattered beams from Ni, Ret- $\gamma$ , and Cu (note  $q_\gamma$  and  $P_\gamma$ ).

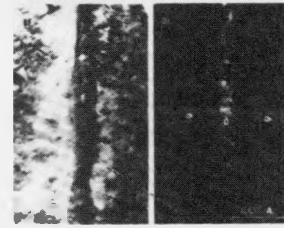
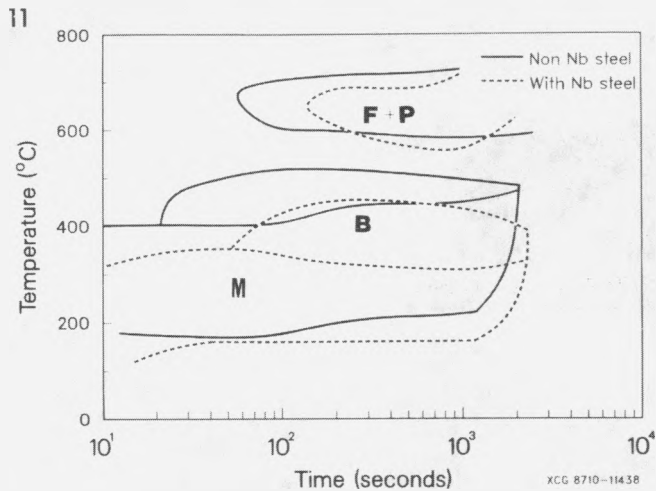


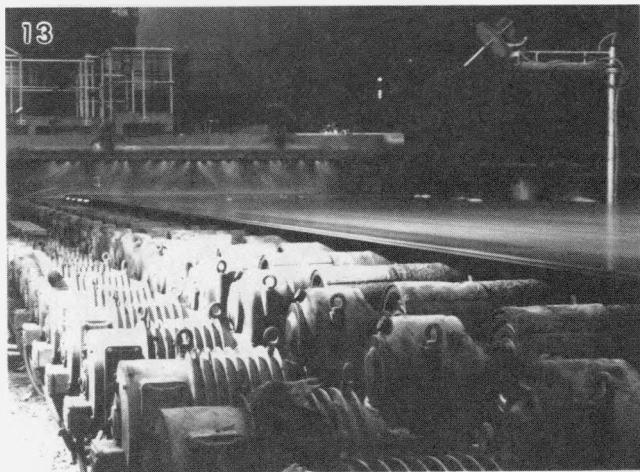
FIGURE 4 - (a) DF and (b) DF TEM images reveal the extent of deformation of Ret- $\gamma$ . (c) Concentration profiles for C, Cr, and Mn over Ret- $\gamma$  film by APA from 1.25C-10Cr-20Ni steel.

XBB 817-7029

Fig. 9 Summary of research on microscopy and microanalysis of the microcomposite steels. FAP analysis proves carbon partitioning to austenite occurs during the martensite (or bainite) reaction.



XCG 8710-11438



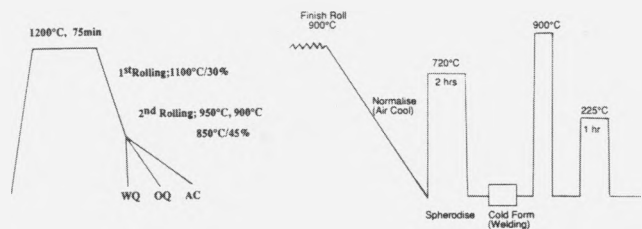
XBB 889-8749

12

	Toughening Mechanism	Results
Conventional Microalloying	<p>Finish Rolling <math>&gt; \gamma_{RC}</math></p> <p>Nb(C,N)</p> <p>Finish Rolling <math>&lt; \gamma_{RC}</math></p>	<p>Good <math>C_v</math></p> <p>Poor <math>K_C</math></p> <p>Moderate Strength</p>
Microcomposite Microalloying	<p>Finish Rolling <math>&gt; \gamma_{RC}</math></p> <p>Quenching</p>	<p>Good <math>C_v</math></p> <p>Expecting Excellent <math>K_C</math></p> <p>High Strength</p>

XBL 881-213

14



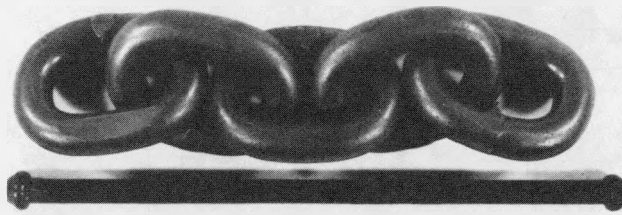
XBL 881-217

Fig. 11 CCT diagram for Fe/2Cr/1Mn/0.26C steel with and without 0.02wt% Nb. (Courtesy ref. 17)

Fig. 12 Schematic diagram to show basis of current control rolling procedure compared to conventional microalloyed steel rolling practice. (Courtesy ref. 17)

Fig. 13 Photograph of plate on the finish line after controlled rolling and accelerated cooling. (Courtesy Dr. J. Humbert, Dillinger-Huttenwerke, West Germany)

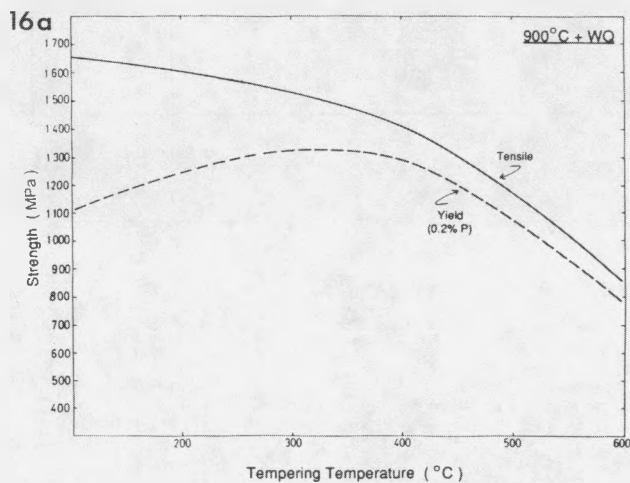
Fig. 14 Processing schemes for (left) control rolling and cooling to produce autotempered lath martensite microcomposites on line, and (right) processing for subsequent cold forming products. Notice the short spherodising time required. (Courtesy ref. 17)



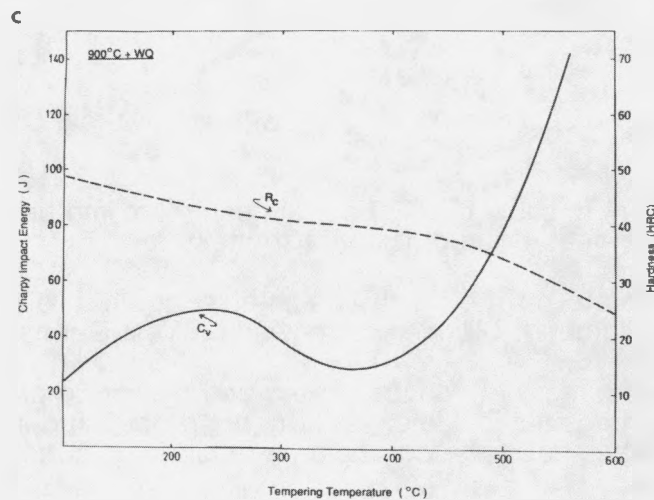
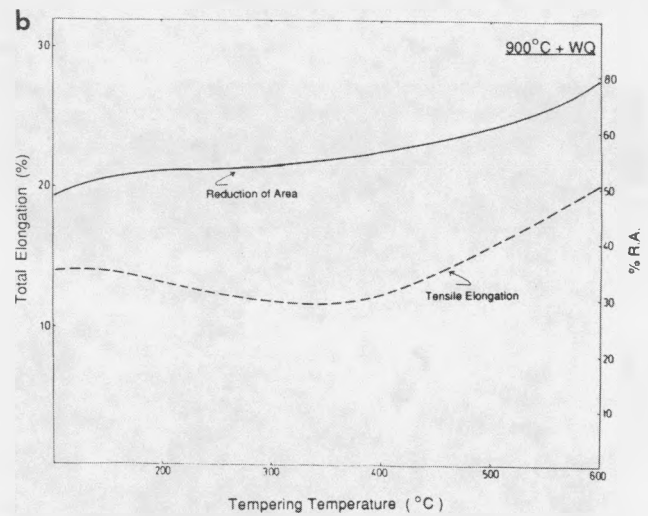
XBB 870-10666

Fig. 15 Examples of cold formed and Q+T chain produced as shown in fig. 14 (RHS) and warm headed retaining bar e.g. for concrete railway sleepers. (Courtesy ref. 17)

Fig. 16 (a,b,c) Strength, total elongation and Charpy values for Fe/2Cr/1Mn/0.15C steel processed as shown in fig. 14 (RHS); quenched and tempered 1 hr. at the temperature shown. (Courtesy ref. 17)

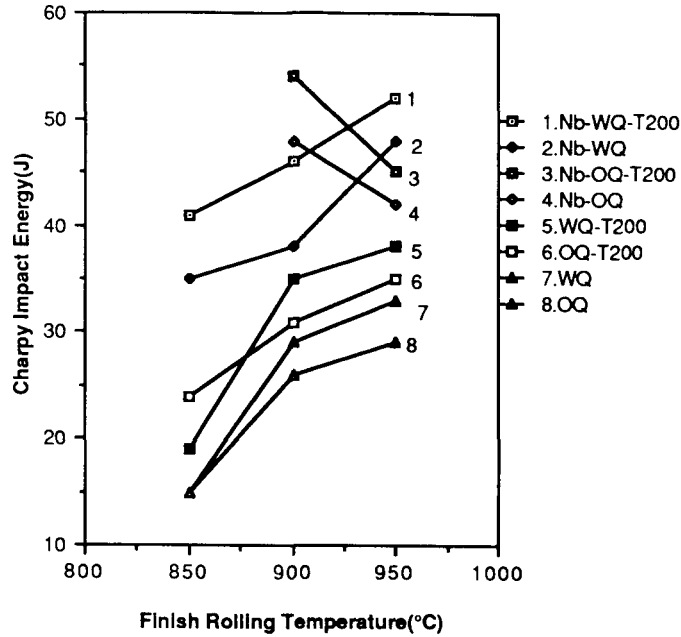


XBL 881-212



XBL 881-210

17

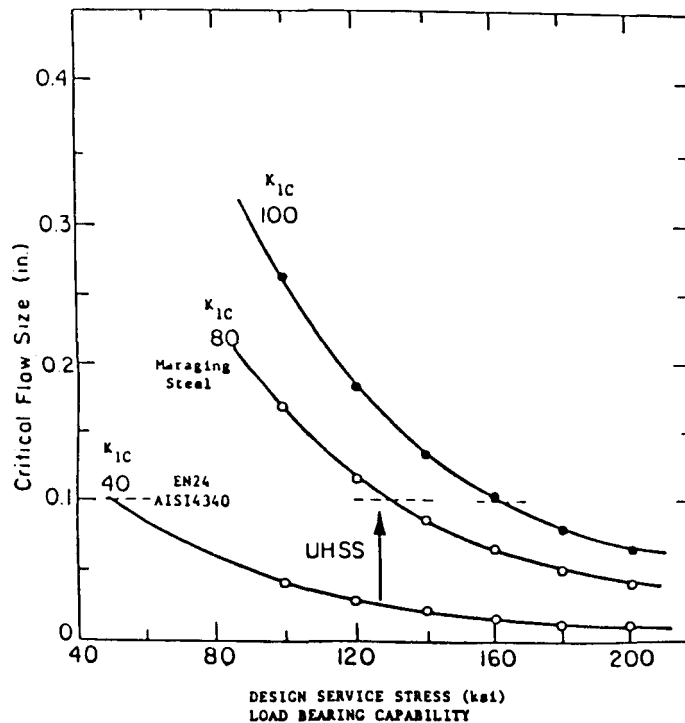


XBL 881-216

Fig. 17 Effect of finish rolling temperatures on Charpy values for Fe/2Cr/1Mn/0.25C steel with and without 0.02Nb processed as shown in fig. 14 (LHS), some tempered at 200°C for 1 hr. (T200). (Courtesy ref. 17)

Fig. 18 Plot of critical flaw size vs. service stress for two commercial steels and a quenched and tempered Fe/4Cr/1Mn/0.3C steel. Control rolled and cooled steels have even higher  $K_{IC}$  values (see fig. 6). ( After ref. 1)

18



XBL 8510-4149A